Cement & Concrete Composites 30 (2008) 557–565

Contents lists available at ScienceDirect

Cement & Concrete Composites

journal homepage: www.elsevier.com/locate/cemconcomp

Capillary pressure in fresh cement-based materials and identification of the air entry value

Volker Slowik *, Markus Schmidt, Roberto Fritzsch

Civil Engineering Department, Leipzig University of Applied Sciences, Germany

ARTICLE INFO

Article history:
Received 29 January 2007
Received in revised form 26 March 2008
Accepted 27 March 2008
Available online 8 April 2008

Keywords:
Plastic shrinkage
Early age cracking
Capillary pressure
Concrete curing
Electrical conductivity

ABSTRACT

Plastic shrinkage in fresh cement-based materials is caused by capillary pressure in the pore system. Within the first few hours after casting, evaporation results in the loss of water and possibly in the formation of menisci in the water surface between the superficial solid particles. With decreasing radius of the menisci the capillary water pressure rises. At a certain pressure, the system becomes unstable and air penetrates into the system. This event is called air entry and assumed to be the origin of strain localization and, consequently, of early age cracking. Similar phenomena may be observed in inert materials. If the capillary pressure is kept below the air entry value by a closed-loop controlled concrete rewetting, the risk of early age cracking is reduced significantly. Experimental results of capillary pressure, deformation and electrical conductivity measurements are presented and a technique for the identification of the air entry value is proposed.

1. Introduction

In concrete structures, cracking may occur even before the material has reached a significant strength, i.e. within the first about 6 h after casting. The reason is the so-called capillary shrinkage. It is often referred to as plastic shrinkage since it takes place in the plastic stage of cement-based materials. Typical damage patterns are meshed or parallel cracks which may often be found in floors or slabs. Fig. 1 shows a concrete slab on grade with a thickness of 25 cm. Characteristic early age cracks with widths of up to 1 mm were formed within the first 4 h after casting when the material was still in its plastic stage. Such early age cracks occur predominantly under high water evaporation rates.

The length of plastic shrinkage cracks varies between 50 mm and 1000 mm and the crack spacing between 50 mm and 700 mm [1]. The corresponding crack width may reach up to 2 mm [2]. Usually, the crack depth is larger then the one of drying cracks in hardened concrete; sometimes plastic shrinkage cracks even split the entire cross-section of a structural component.

The early age cracking risk is mainly influenced by the evaporation rate which depends on air and concrete temperature, wind speed and relative humidity. Other influences are the concrete composition, the specimen geometry, the casting conditions and constraints caused by mechanical boundary conditions or reinforcement. In some cases, the cracks have the same pattern as the reinforcement [3].

It has to be taken into account that surface cracks in concrete structures are in numerous cases caused by multiple effects. In addition to the early age effects, internal and external constraints during the service life of the structure as well as external loading might contribute into the observed crack pattern.

2. Capillary pressure build-up and early age cracking

The physical process leading to plastic shrinkage of cementitious materials is the build-up of a hydraulic pressure in the liquid phase of the material [3–6]. Chemical reactions do not have a decisive influence on this early age process. Similar phenomena may be observed in inert materials [5]. Fig. 2 illustrates the process of capillary pressure build-up and plastic shrinkage. After casting, the solid particles in the fresh concrete settle and water accumulates on the surface where it forms a thin film (Fig. 2A). This effect is called bleeding. The spaces between the solid cement particles, the aggregates and the additives form a system of interconnected pores in this stadium and are almost completely filled with water. Entrapped or entrained air does not play a significant role in the process of early age cracking. Due to evaporation or in certain materials also due to self-desiccation, the thickness of the water film at the concrete surface is reduced. Eventually, the particles at the surface are no longer covered by the water. As a result of adhesive forces and surface tension, water menisci are formed between the solid particles (Fig. 2B). The curvature of the water surface causes a negative pressure in the capillary water. According to the Gauss–Laplace equation, the pressure value p is inversely

* Corresponding author. Tel.: +49 341 3076 6261; fax: +49 341 3076 7045.
E-mail address: slowik@fbb.htwk-leipzig.de (V. Slowik).

0958-9465/$ - see front matter © 2008 Elsevier Ltd. All rights reserved.
doi:10.1016/j.cemconcomp.2008.03.002

Fig. 1. Early age cracks, occurrence within the first 4 h after casting, crack spacing approximately 1 m.

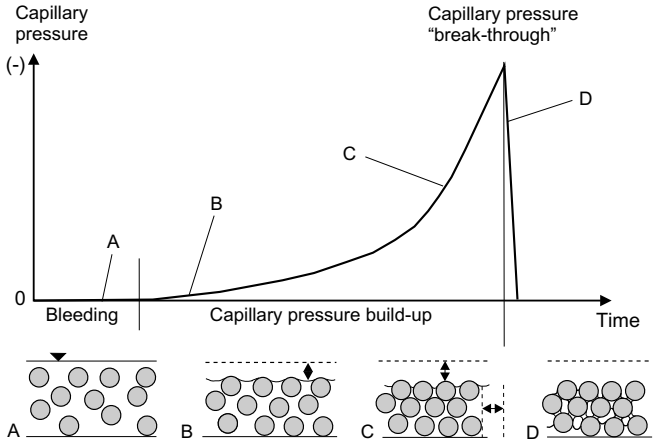

Fig. 2. Capillary pressure build-up in a drying suspension.

proportional to the main radii R of the water surface and also dependent on the surface tension γ of the liquid.

$$p = -\gamma\left(\frac{1}{R_1}+\frac{1}{R_2}\right).$$

This pressure acts on the solid particles resulting in the contraction of the still plastic material [7]. The pores get smaller under the action of the capillary pressure and more pore water is drawn to the surface. Since a part of the pressure is counteracted by repulsive forces between the solid particles, the amount of water transported to the surface is not enough to completely relieve the pressure. The latter is nearly uniformly distributed in the vicinity of the surface where evaporation takes place. Hydrostatic pressure differences are small when compared to the occurring capillary pressure. In the investigations presented here, up to a depth of 10 cm almost uniform pressure values have been measured.

The ongoing evaporation at the surface causes a continuing reduction of the main radii of the menisci (Fig. 2C) resulting in an increase of the absolute capillary pressure value as well as of the shrinkage strain. Fig. 3 shows the development of the capillary pressure in cement paste and the corresponding shrinkage strain during the first 12 h after casting. If the shrinkage is hindered and the cohesive forces between the particles are overcome cracks are formed.

After reaching a certain pressure value, the main radii of the water menisci are too small to bridge all the spaces between the

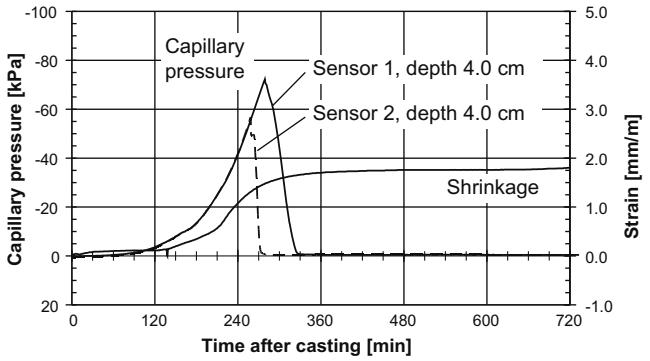

Fig. 3. Capillary pressure and shrinkage strain in cement paste with CEM I 32.5 R versus time, specimen thickness 6 cm.

particles at the surface. If the pressure reaches this limit value, air penetrates the pore system, starting at the largest pores. The system becomes unstable and a relocation of the water in the system takes place. The capillary pressure locally "breaks through" and the pores are no longer completely filled with water (Fig. 2D). However, the solid particles remain interconnected by water sleeves [4].

The penetration of air into the pore system starts locally. Due to the irregular arrangement of solid particles having different size not all the spaces between the superficial particles, i.e. between the particles at the surface, are drained simultaneously. The beginning of this process is the so-called air entry and the pressure reached at air entry is in the following referred to as air entry value. This term is also used in soil mechanics describing a similar phenomenon [8–10].

After air entry, the negative capillary pressure in the pore water continues to rise. Therefore, this event, i.e. the air entry, cannot be identified by a local measurement of the water pressure. In Fig. 3, pressure–time curves measured in the same depth but at different positions are shown. As long as all the sensors are in contact with the pore water they measure exactly the same pressure. However, the pressure values do not collapse simultaneously demonstrating that the penetration of air into the pore system occurs locally.

The water sleeves between the particles in air penetrated regions still cause contracting forces. However, the development of these forces does not resemble the continuing comparably strong capillary pressure build-up. This is due to the fact that on one hand the water pressure in the sleeves increases with decreasing surface radius and on the other hand the area on which this pressure is acting diminishes.

When air starts to penetrate the pores, i.e. when the pressure reaches the air entry value, the plastic cracking risk is assumed to reach its maximum because the drained pores are weak points in the system [11]. The contracting forces between the particles in the air penetrated regions are considerably smaller than those in the water filled regions. Hence, a localization of strains is taking place possibly leading to visible cracks. This may be illustrated by electron microscopic images of a drying suspension made of fly ash and water, see Fig. 4 from the left to the right. In the first two images, all the particles at the surface are surrounded by the water front. In the second image, however, the evaporation had already led to a descent of the water level between the solid particles. After continuous drying, the third image was taken. Some dark spots may be seen in the right half of this image. At these positions, air had penetrated the pores. The fourth image which was taken shortly after the third one shows a crack which was formed obviously along a line connecting the air penetrated pores. The latter were presumably "weak points" from the mechanical point of view.

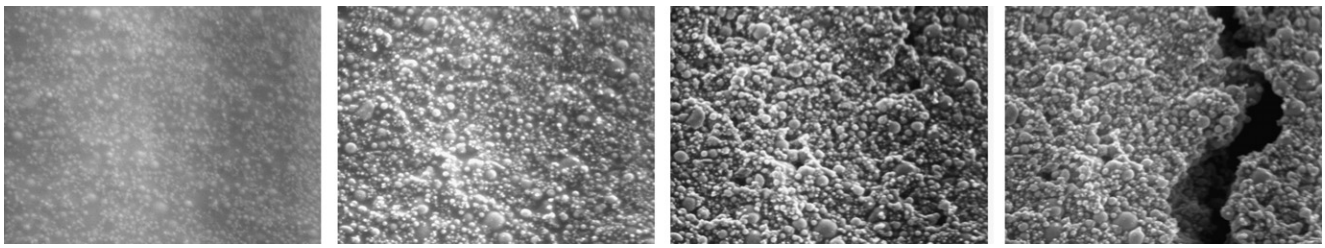

Fig. 4. Electron microscopic images of a drying suspension of fly ash and water, magnification factor 300.

It has to be pointed out that reaching the air entry value does not necessarily result in cracking. Cohesive stresses between the particles resulting from hindered shrinkage strain and sufficient particle mobility are also required. However, cracking is impossible without air entry into the drying suspension.

A correlation of air entry and crack formation has been also found in soil mechanics. Peron et al. [10] investigated the desiccation of sandy silt by experimental means. Free as well as constrained drying shrinkage tests were performed. In the case of the constrained tests cracking occurred at a capillary pressure which was close to the air entry value of the material. It was suggested that stress generation in the drying soil is controlled by the constrained shrinkage strains whereas crack initiation is interconnected with the air entry.

The development of the capillary pressure in the fresh material is not only dependent on the water evaporation rate but also on the particle size distribution. The smaller the spaces between the particles the steeper the pressure rise for a given evaporation rate. The air entry value is a specific property of the material [8–10]. Based on the physical explanation of capillary pressure build-up it may be concluded that this value depends on the particle size distribution, on the water–solid ratio, on the air content as well as on the mobility of the particles. Some compositions of high performance concrete are characterized by small particle sizes, high binder content and low water–cement ratio intensifying self-desiccation. These characteristics may lead to comparably high absolute values of capillary pressure and shrinkage strain resulting in an increased early age cracking risk.

Subject of the study presented here is the air entry value. If this value could be identified for a certain material, it might be used as a threshold pressure for preventing plastic shrinkage cracking. Following this idea, a method of concrete curing based on in situ capillary pressure measurement and closed-loop controlled rewetting of fresh concrete surfaces has been proposed [12]. It allows to significantly reduce the early age cracking risk. If the capillary pressure reaches a previously defined threshold, the absolute value of which should be lower than the one of the air entry value, the concrete surface is rewetted. Thereby, the negative capillary pressure is reduced temporarily but not completely relieved, see Fig. 5. The controlled rewetting does not create a continuous water film on the concrete surface which might degrade the near-surface material properties due to an increased water–cement ratio. By using commercial fogging equipment the proposed curing method has been tested under site conditions [12]. The work presented here was motivated by the necessity to identify a critical capillary pressure value for a specific material composition.

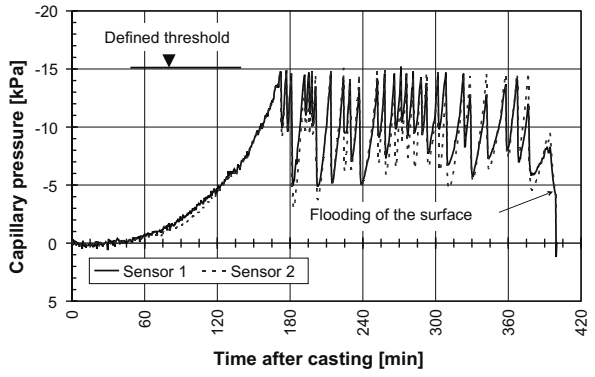

Fig. 5. Capillary pressure versus time during controlled surface rewetting of a cement paste specimen.

The proposed closed-loop controlled concrete curing provides an alternative to the monitoring of the evaporation rate, for instance by using a curing meter [13] which indirectly gives information on the cracking risk. Since the proposed method is based on the in situ measurement of capillary pressure and on the material specific air entry value it allows a more direct and presumably a more reliable control of the early age cracking risk.

As explained before, the local measurement of the capillary pressure does not allow the identification of the air entry value. A more integral indicator was sought after and deformations as well as electrical conductivity were found to be suitable measurands for the problem to be solved here. Electrical conductivity measurements have been undertaken for investigating different chemical and physical processes taking place in cementitious materials [14–16]. This physical property is influenced by a number of factors and it appears to be nearly impossible to separate and quantify the different effects, especially in fresh concrete. However, it was expected that a discrete event like the air entry would become apparent in a continuous electrical conductivity measurement. Since the particles after air entry are at some locations interconnected by the water sleeves only, the electrical conductivity should be noticeably lower than in the water saturated stage.

In soil mechanics, the air entry value is usually determined on the basis of degree of saturation versus suction curves [9]. These curves are determined experimentally by repeatedly measuring the water content of a soil sample while incrementally increasing the pressure difference between the pore water and the surrounding air. Since these experiments require a comparably long test time, they are not applicable for cementitious materials which are characterized by evolving material properties due to chemical reactions.

In the following, experiments performed with early age cementitious materials as well as with fly ash are reported and the identification of the air entry value is shown. These investigations were aimed towards a better understanding of the material behavior of early age concrete and towards technical possibilities for minimizing the early age cracking risk.

3. Experiments

3.1. Materials

In order to eliminate chemical effects due to cement hydration different inert materials were investigated in addition to cement

Table 1
Material properties

	Fly ash	Cement CEM I 32.5 R	Cement CEM I 42.5 R
Specific surface (Blaine; cm^2/g)	4500	2610	3650
Water consumption[a] (% per mass, related to cement mass)	–	26.5	29.7
Beginning of setting[a] (min)	–	160	150
End of setting[a] (min)	–	210	200

[a] According to DIN EN 196-3:2005; determination of setting time and soundness.

paste and concrete. In this way, the physical phenomena occurring during drying could be studied separately.

Of special interest is the behavior of fly ash which has been a subject of the experimental investigations as a "model material". The particle size distribution roughly resembles the one of cement. Furthermore, the fly ash particles have a spherical shape. For that reason, particle interlocking during shrinkage is expected to be of minor importance. This simplifies the interpretation of the experimental findings. Table 1 shows the most important properties of the materials included in the experimental investigations.

3.2. Experimental set-up and sensors

The experiments were conducted in two plastic forms having the same geometry of $30 \times 30 \times 10\,cm^3$, see Fig. 6. In the form shown in Fig. 6a, two LVDTs served for measuring the horizontal displacement between the form and markers embedded in the sample at opposite sides. In the rectangular horizontal direction, identical horizontal displacements were assumed because of the quadratic base of the form. An additional LVDT was arranged vertically for measuring the settlement at the specimen surface. Its sensor tip touched a $2 \times 2\,cm^2$ wide metallic wire lattice which has been applied to the specimen surface. In this way, the settlement may be measured directly at the surface of the superficial particles [17]. Penetration of the sensor tip as well as floating of the sensor target is prevented. All LVDTs used in the experiments did not have a spring driven tip in order to avoid unintended loading.

In addition to the horizontal shrinkage and to the settlement, the electrical conductivity, the capillary pressure, the mass loss, the specimen temperature as well as the climatic conditions, specifically air temperature and relative humidity, were measured. The measurement of electrical conductivity and capillary pressure were undertaken at a different specimen, see Fig. 6b, in order to eliminate displacement hindrance by the embedded sensors. Despite simultaneous placement and drying of the material in both forms, there might have been slight differences in the behavior of the samples due to the variation of the local material properties.

The electrical conductivity as the reciprocal of the electrical resistance was measured by using a sensor which has been especially designed and fabricated for this purpose. A similar sensor was proposed before by Schießl et al. [16] for the application to hardened concrete. The sensor used here consists of a hollow polyvinylchloride cylinder with several identical ring-shaped stainless steel electrodes arranged parallel to the specimen surface in different depth, see Fig. 6b. By successively measuring the electrical resistance between pairs of neighboring rings a depth dependent conductivity profile is obtained. It has been found that the investigation of the drying process and especially of the air entry value requires a depth sensitive electrical conductivity measurement. With the sensor used here, the electrical conductivity may be measured up to values of 50 mS at seven positions in a distance from the specimen surface between 5 mm and 40 mm. An alternating voltage with 20 mV amplitude and a frequency of 2 kHz is used. Since only qualitative conclusions are to be drawn on the basis of the electrical conductivity, a complicated correction of the measured values with respect to chemical influences, for instance changing ion concentrations in the pore solutions, or with respect to the temperature is not required. The electrical conductivity measurement was solely aimed to the identification of the air entry value.

The capillary pressure was measured by small-sized electric pressure sensors connected to the pore system by 20 cm long brass tubes having an inside diameter of 3 mm, see Fig. 6b. The tubes were completely filled with de-ionized and to a large extend outgassed water. They were arranged horizontally in a distance of 4 cm from the specimen surface, i.e. approximately in the depth of the deepest electrode of the conductivity sensor. The distance between the electrical conductivity sensor and other conductive fixtures in the specimen, for instance the brass tubes or the thermo-couples, was always larger than 10 cm ensuring that the other sensors would not significantly influence the conductivity measurement. Both the conductivity sensor and the tips of the pressure sensors were located at about the same distance from the vertical specimen side faces. All smooth inside surfaces of the plastic forms were lubricated with a release agent for minimizing frictional forces.

Depending on the investigated material, the duration of the experiments was between 20 h and 48 h. During the experiments, the samples were stored under constant temperature and relative humidity. It was found that comparably small changes in the evaporation rate or in the water content of the material noticeably influence the capillary pressure versus time curve.

3.3. Experimental program

Table 2 contains the conditions under which experiments have been performed. Most of the tests were conducted repeatedly. The influence of the specimen thickness on the capillary pressure has been investigated and discussed before [5] and will not be a subject of the present paper.

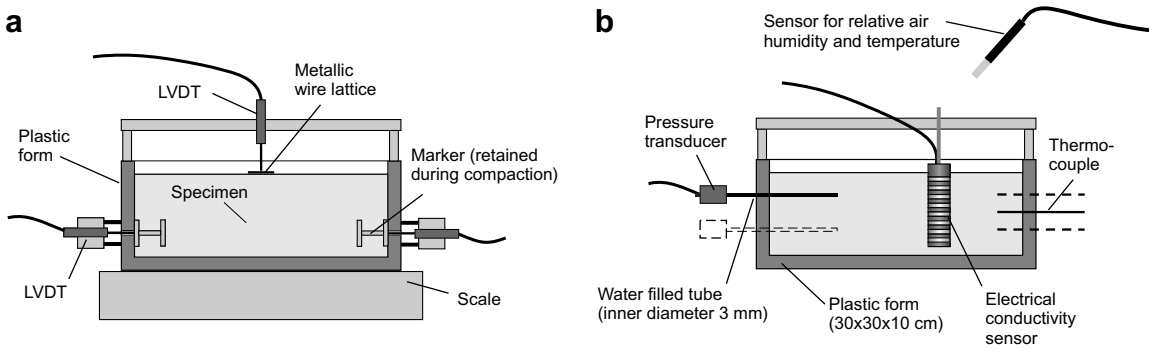

Fig. 6. Experimental set-up with two forms used in parallel.

Table 2
Test conditions

Material	Water–solid ratio	Climatic conditions	Specimen thickness (cm)
Fly ash	0.250	45% RH/20 °C	6, 8, 10
CEM I 32.5 R	0.263	45% RH/20 °C	6
CEM I 42.5 R	0.269	45% RH/20 °C	6
Concrete	0.41 (water–binder ratio)	30% RH/22 °C air current 4.8 m/s	6

RH, relative air humidity.

The material was prepared in a mortar mixer with 7 l capacity. Consequently, the mixer had to be filled twice for preparing the two specimens required for one experiment. Solid material and water were consecutively given into the wet mixer and slowly distributed. It followed a 3 min mixing period at moderate speed. Then, the material was cast into the forms in a single layer and compacted on a vibrating table in two periods of 10 s each. The measurement started between 25 min and 30 min after the beginning of the mixing.

In preliminary tests, the material compositions were adjusted in a way that only a thin water layer on the specimen surface was formed by slight bleeding. This resulted in the water–solid ratios given in Table 2.

4. Experimental results and discussion

4.1. Experiments with fly ash

In the beginning, the physical effects to be investigated were studied on inert materials. The results of the experiments conducted with fly ash will be presented in the following.

Early age deformations may be subdivided into one-dimensional settlement and three-dimensional capillary shrinkage. Initially, gravitation leads to a subsidence of the particles. Water is pushed out of the spaces between the particles and accumulates at the specimen surface where it evaporates. For the given environmental conditions (20 °C, 45% relative air humidity), the water mass loss due to evaporation is linear in time, see Fig. 7a. The evaporation rate amounts to approximately 0.145 kg/(m^2 h) here. Fig. 7b shows the deformations and the capillary pressure. A comparably large initial settlement may be seen. It stagnates for some time and starts again with the capillary pressure build-up, however, at a lower rate. The slight decrease after the intense initial settlement has been observed in all the experiments but cannot yet be explained satisfactorily. When the available water cannot cover all the particles any longer, the formation of menisci between the solid particles at the surface starts. Consequently, capillary pressure is built up in the pore system resulting in contracting forces and shrinkage.

In the experiment chosen for Fig. 7, the capillary pressure build-up started about 90 min after casting. If the contracting forces are large enough to overcome the adhesion between formwork and specimen, horizontal shrinkage deformations may be measured. Here, this happened after about 480 min, see Fig. 7b. When horizontal shrinkage deformations start, the slope of the settlement versus time curve decreases. Horizontal contraction of the material results in a reduction of the settlement rate.

The beginning of the horizontal displacement is accompanied by discontinuities in the capillary pressure curve, see Fig. 7b. This effect was observed in almost all the experiments conducted with fly ash and may probably be attributed to the successive debonding from the form.

The settlement reaches a characteristic temporary maximum after 740 min, see Fig. 7b. Afterwards it slightly decreases while the horizontal shrinkage strain further increases. This maximum in the settlement curve is attributed to the air entry. At the flanks of the drained regions, the resulting capillary forces on the particles tend to change their orientation into a horizontal direction. As a result, horizontal shrinkage increases locally and a portion of the settlement is relieved. This happened, see Fig. 7b, when the capillary pressure amounted to about −53 kPa which is considered to be the air entry value.

Fig. 8 shows the results of electrical conductivity measurements for the same experiment already used for Fig. 7. Before air entry, electric current is transmitted almost completely through the water in the saturated pore system. The electrical conductivity is thereby dependent on the electrolyte concentration in the pore water, on the temperature as well as on the pore structure and on the sensor geometry [14]. With the sensor used here, in a fly ash suspension after casting conductivity values between 10 mS and 20 mS were measured. This corresponds to an electrical resistance between 50 Ω and 100 Ω. For a graphical presentation of the physical effects due to water evaporation, the resistance appears to be a more suitable quantity as compared to conductivity since it strongly increases during the drying of the material.

Fig. 8a shows resistance curves obtained in different depths. In the beginning, the resistance values exhibit only slight deviations. The latter may be explained by material inhomogeneity and boundary effects from the specimen surface. Within the first 2 to 3 h after casting, the different resistance curves are almost parallel. In this period the material is consolidated, some bleeding occurs and the capillary pressure starts to develop. The slight resistance increase presumably results from the narrowing of the pore system. About 740 min after casting, a sudden change in the resistance curves is observed. At this moment, the capillary pressure has reached the air entry value. Air penetrates into the pore system

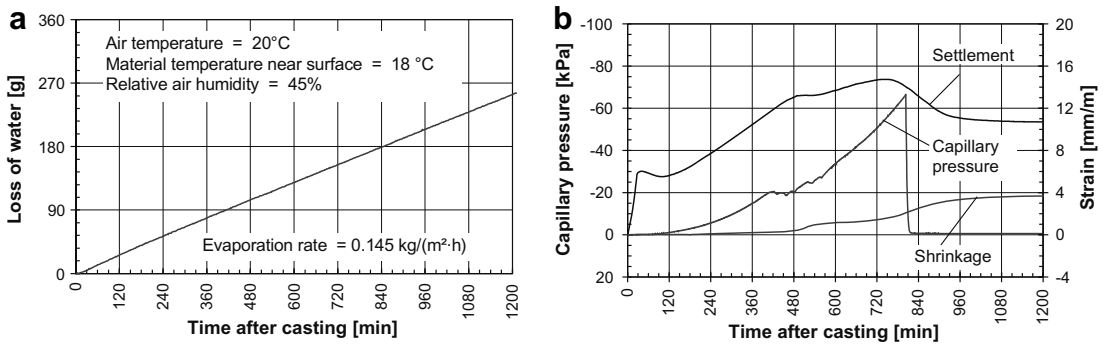

Fig. 7. Water loss (a), capillary pressure and deformations (b) versus time for a drying experiment with fly ash.

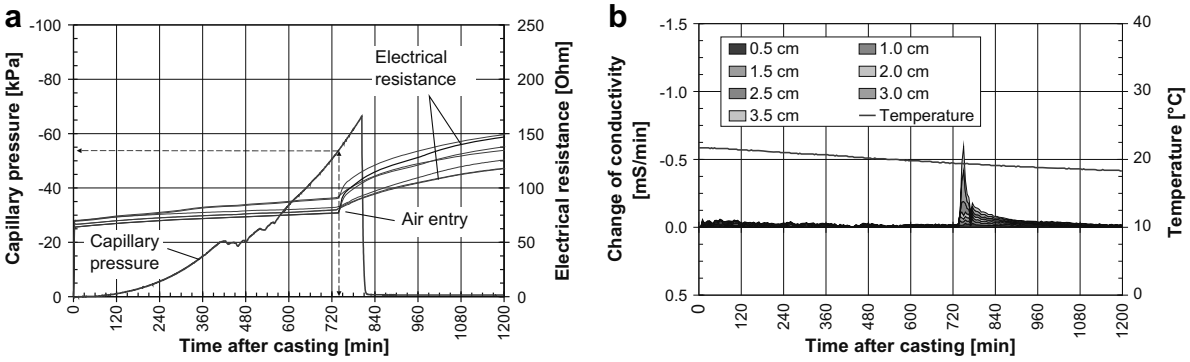

Fig. 8. Capillary pressure, electrical resistance (a) and change of conductivity (b) versus time for a drying experiment with fly ash.

and the water is redistributed. The electrical resistance of the system increases noticeably and quite abruptly by up to 10%. In most cases, this effect is strongest close to the surface and becomes weaker with increasing depth. However, it is detectable usually over the whole sensor range of 4 cm and it allows identification of the air entry value. It has to be pointed out that the electrical conductivity sensor causes some mechanical constraint on the material. This might promote air entry in the vicinity of the sensor. However, the air entry value detected by electrical conductivity measurements is in good accordance with the one determined on the basis of deformation measurements. Therefore, the sensor is not expected to significantly influence the air entry value by constraining shrinkage deformations. In none of the experiments, visible cracks were observed in the vicinity of the electrical conductivity sensor.

Sometimes, the resistance increase is not as pronounced as in Fig. 8a or there is a slight time shift between the events of abrupt rise in different depth. In these cases, the slope of the conductivity or resistance curves might help to identify the air entry value. In the corresponding graphs, see Fig. 8b, even a cluster of comparably small events of sudden resistance increase may be detected reliably.

The experimental results show that the air entry is not necessarily accompanied by a capillary pressure break-through, see Fig. 8a. The pressure in the water remaining in the pore system continues to rise.

After air entry, the electrical resistance increases with a depth dependent rate. Because of the emerging moisture gradient, the resistance curves show a characteristic diversification. Sudden resistance changes as the one at the air entry were thereafter not observed again.

4.2. Experiments with cement paste and concrete

In cement paste, generally the same effects like in fly ash could be observed. However, the capillary pressure build-up starts earlier. This may be attributed mainly to the different pore structure and to the additional loss of pore water due to cement hydration. Fig. 9 shows experimental results obtained for cement paste with CEM I 32.5 R (left column) and CEM I 42.5 R (right column), respectively.

The initial electrical conductivity in the cement paste was in the range between 30 mS and 50 mS corresponding to 20 Ω and 40 Ω, respectively, see Fig. 9a and b. In the beginning of the measurement, only small changes of the electrical conductivity are observed. The chemical reaction rate is low in this phase. As in the case of fly ash, the air entry is accompanied by a comparably strong change of the electrical conductivity, see Fig. 9c and d. However, this event occurs earlier than in the case of fly ash, in the experiments selected for Fig. 9 after about 185 min for CEM I 32.5 R and after about 125 min for CEM I 42.5 R.

In contrast to the experiments performed with fly ash, the cement paste shows a strong electrical resistance increase about 7–10 h after casting. This may be attributed to the changes in the microstructure or in the pore water properties due to hydration.

The vertical deformation, i.e. the settlement, of the cement paste reaches a maximum at the time of air entry and slightly decreases afterwards, as also observed for fly ash. In the horizontal direction, the shrinkage strain continues to increase after the air entry, see Fig. 9e and f. The ascending vertical displacement between 6 h and 10 h after casting may be explained by thermal expansion due to hydration heat.

Starting with the capillary pressure build-up, the volume change of the specimen resulting from vertical and horizontal strain, see Fig. 9g and h, is equal to the volume of the evaporated water. The latter has been determined on the basis of the measured mass loss. After air entry, the volume of the specimen does not decrease anymore while water continues to evaporate. It is assumed that after air entry the volume of the air penetrating into the material causes this deviation of the specimen volume change from the evaporated water volume. In addition, the consolidation of the particle structure as well as the development of the cement paste microstructure prevents further plastic shrinkage.

The behavior of concrete was found to be similar to the one of cement paste. Fig. 10 contains the results of an individual experiment performed under high water evaporation rate. The concrete used here had a maximum aggregate size of 16 mm, a water–binder ratio of 0.41 and contained 440 kg/m^3 of CEM I 32.5 R. The same cement as in the experiments with cement paste was used. After about 70 min, the characteristic maximum of the settlement, see Fig. 10a, and the deviation of the volume change curve from the water loss curve, see Fig. 10c, were observed. Detecting the air entry value on the basis of electrical conductivity measurements also appeared to be possible. However, the characteristic increase in electrical resistance, see Fig. 10b and d, was detected about 20 min after the deformation measurements indicated air entry. It has to be considered that deformation and conductivity measurements were performed in different forms, see Fig. 6, although the material originated from the same batch. In the experiment used for Fig. 10, the air entry value amounted to about −10 kPa.

It was found that the air entry values of concrete and cement paste are approximately in the same order of magnitude. This results from the fact that the pore diameters controlling the capillary pressure build-up are in the cement paste the same as in the cement matrix of the concrete.

For the following discussion, axially symmetric open pores at the specimen surface are assumed. Their axes are oriented normal to the surface. The diameter of such a pore is varying with the

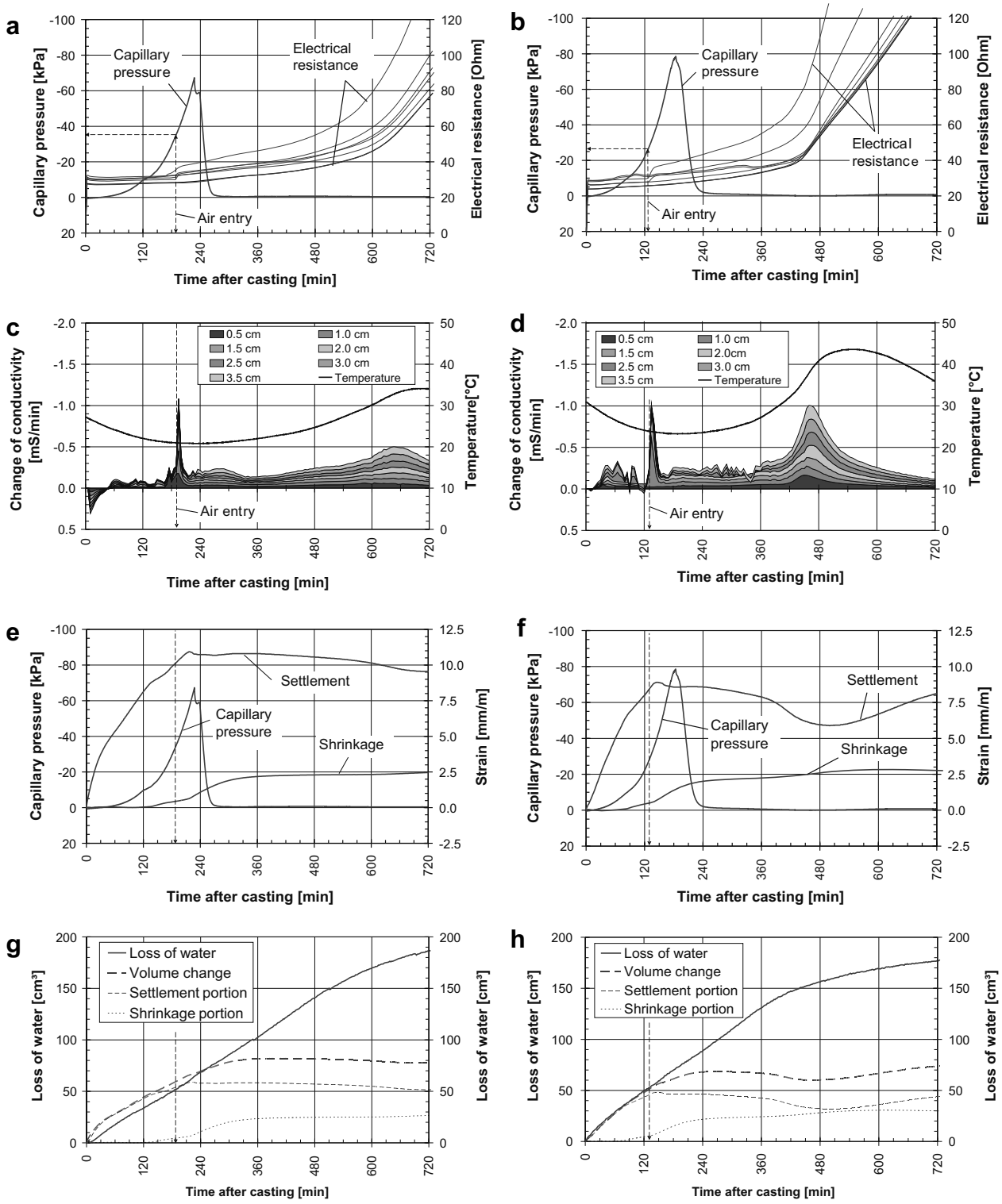

Fig. 9. Experimental results obtained for cement paste with CEM I 32.5 R (left column) and CEM I 42.5 R (right column), cement properties according to Table 1, water–cement ratio according to Table 2.

depth, i.e. with the distance from the surface, and has a minimum in the vicinity of the surface. Under these assumptions, the capillary pressure at air entry is inversely proportional to the minimum diameter of the biggest pore, in the following referred to as equivalent pore diameter. The curve in Fig. 11 shows this relationship which results from the Gauss–Laplace equation for an axially symmetric capillary given in the same diagram. When the radius of the meniscus reaches one half of the equivalent pore diameter, air penetrates into the pore system and the corresponding pressure is equal to the air entry value. Because of the non-linearity of the applied equation, the comparably large variation of the air entry value for fly ash corresponds to a narrow distribution of the equivalent pore diameter. For cement paste and concrete, the air entry value was found to be in the range between −10 kPa and

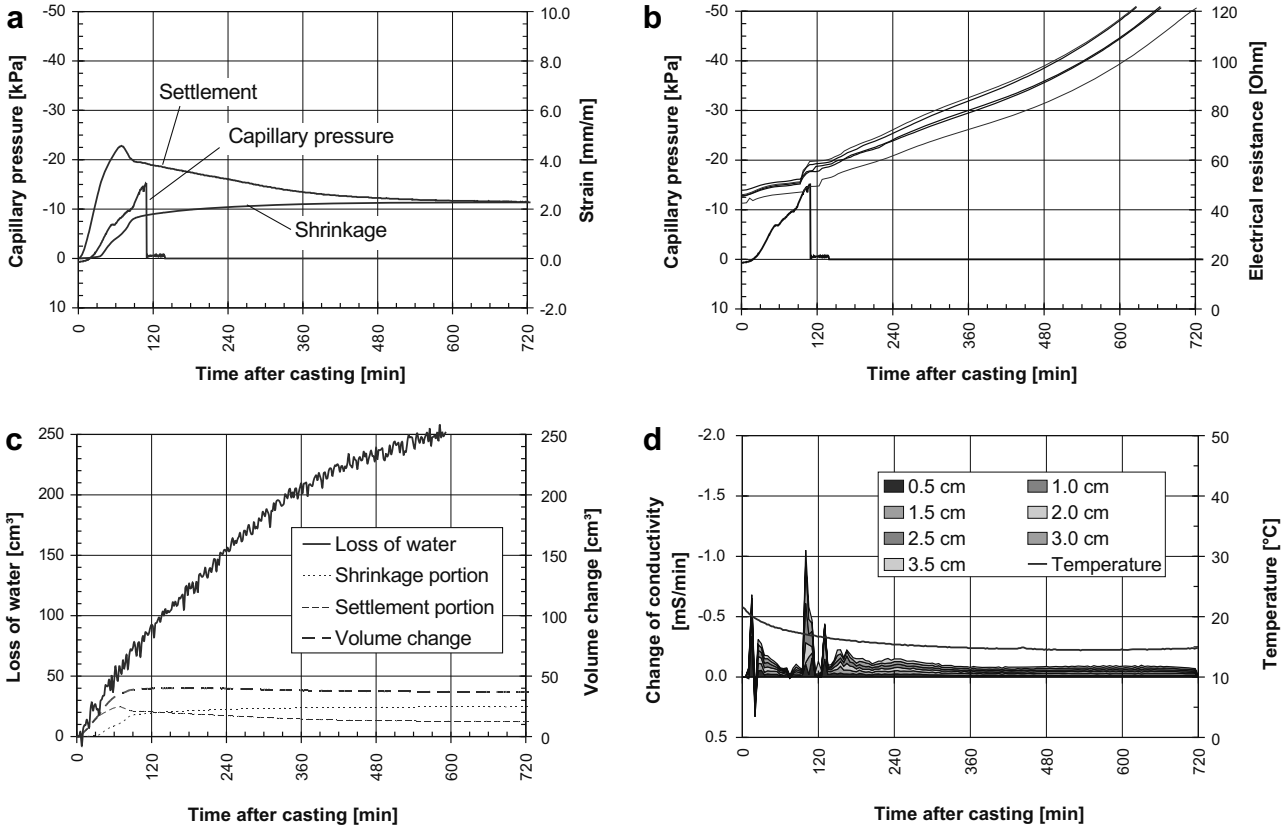

Fig. 10. Experimental results obtained for concrete with 440 kg/m^3 CEM I 32.5 R and a maximum aggregate size of 16 mm, cement properties according to Table 1, water–cement ratio according to Table 2.

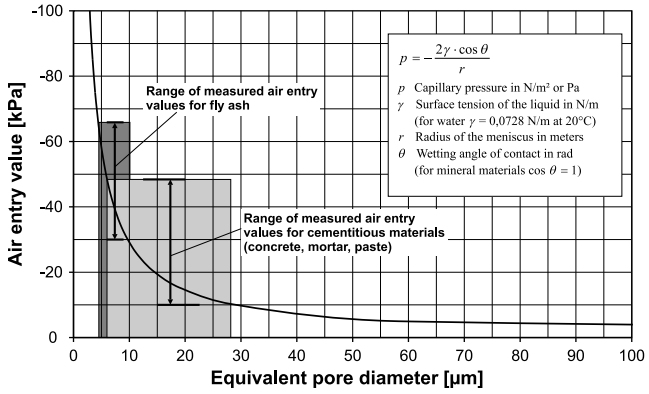

Fig. 11. Air entry value versus equivalent pore diameter for assumed axially symmetric pores and experimentally determined air entry values.

−45 kPa and, consequently, the scatter of the equivalent pore diameter is comparably large.

5. Conclusions

Capillary pressure is the source of shrinkage in the plastic stage of cementitious materials and may eventually lead to cracking. This physical phenomenon may be observed not only in cementitious materials but also in quasi inert materials like fly ash. The capillary pressure build-up depends on the pore structure at the surface as well as on the rate of water loss, normally caused by evaporation. In the process of capillary pressure build-up, the air entry is a characteristic event describing the sudden draining of the largest pores between the particles at the surface and the resulting redistribution of the pore water. It is assumed that at the time of air entry the cracking risk is high since the drained regions at the surface are weak points inducing strain localization. Therefore, the air entry value, i.e. the capillary pressure value at air entry, may serve as an indicator for the risk of early age cracking.

In laboratory experiments, it was found that the air entry is accompanied by a temporary maximum of the settlement, by a beginning deviation between specimen volume change and evaporating water volume as well as by a sudden drop of electrical conductivity.

Knowing the air entry value for a certain material, it is possible to define a capillary threshold pressure which should not be exceeded in concrete processing in order to minimize the risk of early age cracking. This threshold value may be used in a closed-loop controlled concrete curing based on capillary pressure dependent rewetting of the fresh concrete surface.

Acknowledgment

The financial support of the research by the Federal Ministry of Education and Research in Germany is gratefully acknowledged.

References

[1] Kosmatka SH, Kerkhoff B, Panarese WC. Design and control of concrete mixtures. Skokie, (IL): Portland Cement Association; 2002.
[2] Grube H. Ursachen des Schwindens von Beton und Auswirkungen auf Betonbauteile. Schriftenreihe der Zementindustrie, Heft 52. Düsseldorf: Beton Verlag, 1991.

[3] Wittmann FH. Zur Ursache der so genannten Schrumpfrisse. Zement und Beton 1975;85/86:10–6.
[4] Wittmann FH. On the action of capillary pressure in fresh concrete. Cement Concrete Res 1976;6:49–56.
[5] Radocea A. A Study on the mechanism of plastic shrinkage of cement-based materials. PhD Thesis, Göteborg, Chalmers University of Technology Göteborg; 1992.
[6] Lura P, Mazzotta GB, Rajabipour F, Weiss J. Evaporation, settlement, temperature evolution, and development of plastic shrinkage cracks in mortars with shrinkage-reducing admixtures. In: Proceedings of the international RILEM-JCI seminar on concrete durability and service life planning (ConcreteLife'06), Ein-Bokek, Israel; March 14–16, 2006. p. 203–13.
[7] Slowik V, Schlattner E, Klink T. Experimental Investigation into early age shrinkage of cement paste by using fiber Bragg gratings. Cement Concrete Compos 2004;26(5):473–9.
[8] Witte M. Veränderung des Festigkeits- und Verformungsverhaltens bei bindigen Böden aufgrund von Porenwasserspannungen. PhD Thesis. Technische Universität Carolo Wilhelmina zu Braunschweig: Braunschweig; 2003.
[9] Fredlund DG, Rahardjo H. Soil mechanics for unsaturated soils. New York, Chichester, Brisbane, Toronto, Singapore: John Wiley and Sons Inc.; 1993.
[10] Peron H, Laloui L, Hueckel T, Hu L. Experimental study of desiccation of soil. ASCE, Geotechnical Special Pub 2006;147:1073–84.
[11] Hammer TA. The use of pore water pressure to follow the evolution from fresh to hardened concrete. In: Proceedings of the 2nd international symposium on advances in concrete through science and engineering, Quebec City, Canada; September 11–13, 2006.
[12] Schmidt D, Slowik V, Schmidt M, Fritzsch R. Auf Kapillardruckmessung basierende Nachbehandlung von Betonflächen im plastischen Materialzustand (early age concrete curing based on capillary pressure measurement). Beton- und Stahlbetonbau 2007;102(11):789–96.
[13] Jensen OM. Monitoring water loss from fresh concrete. In: Proceedings of the international RILEM-JCI seminar on concrete durability and service life planning (ConcreteLife'06), Ein-Bokek, Israel; March 14–16, 2006. p. 197–202.
[14] McCarter WJ, Curran PN. The electrical response characteristics of setting cement paste. Mag Concrete Res 1984;36(126):42–9.
[15] Schulte C, Mader H, Wittmann FH. Elektrische Leitfähigkeit des Zementsteins bei unterschiedlichem Feuchtigkeitsgehalt. Cement Concrete Res 1978;8:359–68.
[16] Schießl P, Souchon T, Breit W. Berechnungsmodell zur Bestimmung von Feuchtigkeitsgehalten aus Widerstandsmesswerten der multi-ring-Elektrode ermittelt in der Betonrandzone mittels Einbausensoren. Stuttgart: Fraunhofer IRB Verlag; 1997.
[17] Holt EE. Early age autogenous shrinkage of concrete. VTT Publications 446. Espoo: Technical Research Centre of Finland; 2001.